Fission track analysis and trace element compositions of apatite for thermo- and tephrochronology of a Cretaceous event sedimentary sequence on the east Asian convergent margin

In: Horizons in Earth Science Research ISBN: 978-1-53612-831-4
Editors: B. Veress and J. Szigethy

Chapter 7

FISSION TRACK ANALYSIS AND TRACE ELEMENT COMPOSITIONS OF APATITE FOR THERMO- AND TEPHROCHRONOLOGY OF A CRETACEOUS EVENT SEDIMENTARY SEQUENCE ON THE EAST ASIAN CONVERGENT MARGIN

Yasuto Itoh[1,*], Paul F. Green[2], Reishi Takashima[3] and Keiji Takemura[4]

[1]Graduate School of Science, Osaka Prefecture University, Osaka, Japan
[2]Geotrack International, Brunswick West, VIC, Australia
[3]The Center for Academic Resources and Archives (Tohoku University Museum), Tohoku University, Sendai, Japan
[4]Institute for Geothermal Sciences, Kyoto University, Beppu, Japan

[*] Corresponding Author E-mail: yasutokov@yahoo.co.jp.

ABSTRACT

A geochemical and thermochronological study designed for the elucidation of the burial and exhumation history of an extensive pull-apart basin was conducted on the East Eurasian longstanding convergent margin. The trace element compositions of apatite yields from volcanic ashes intercalated in a marine siliciclastic alternating beds of the Izumi Group, which buried a late Cretaceous tectonic basin in southwestern Japan, were determined in this study. It was shown that acidic ashes with a similar appearance can be successfully discriminated using binary plots of selected elements, and a firm basis to compare thermal histories independently reconstructed for selected horizons was established. Apatite fission track (FT) analysis was executed for the same ash samples from two sites, and their anomalous track length distributions were found to be suggestive of tracks having annealed under thermo-tectonic events after initial cooling. In combination with zircon FT ages obtained from five volcanic layers of the host sedimentary sequence, a numerical model for the FT annealing processes indicates the occurrence of two post-depositional cooling (uplift) periods beginning 81–36 Ma (Campanian to Eocene) and 38–18 Ma (late Eocene to early Miocene). The former probably reflects regional contraction episodes exemplified by the K/T gap, whereas the latter is synchronous with the initiation of back arc rifting around the area of the present-day Japan Sea, which inevitably provoked a prevailing uplift.

1. INTRODUCTION

The evolutionary process of convergent margins is an important study theme for geologists because it is key to understanding the dynamics of the material recycling system of the Earth. The East Asian margin is a typical site of tectonic events, such as arc migration, amalgamation, and collision, related to the longstanding subduction of oceanic plates. Itoh and Takashima (2017) recently executed a well-organized paleomagnetic investigation on this margin and found that the present-day island arcs around the northwestern Pacific are a mixture of allochthonous and autochthonous blocks that experienced massive reshuffle under the influence of complex plate motion. Based on their quantitative estimate of the translation history of crustal blocks, Itoh et al. (2017a) presented a

comprehensive plate reconstruction model representing the most probable configuration of the region since 100 Ma. Although this model successfully solves the paradox of the coexistence of multifaceted geodynamic regimes by theorizing the existence of a lost marginal sea plate that transported allochthonous terranes, many ambiguous points remain regarding the timeline of epoch-making events because of insufficient chronological data.

This paper addresses one of the significant unsolved problems of this model: the burial and exhumation history of the Cretaceous sedimentary basins along the East Asian margin, where lateral movements on a longstanding trench-parallel crustal break called the Median Tectonic Line (MTL) forced the generation of an adjoining pull-apart basin. The enormous narrow tectonic depression was buried by marine sediments of the Izumi Group, the depocenter migration of which represents the propagation of the termination of the MTL. Itoh et al. (2017b) applied fission track (FT) thermochronological analysis to turbidite sandstones of the sedimentary unit. They found that the annealing of apatite FT recorded three stages of intermittent cooling (uplift) events from the Cenomanian to late Miocene. Thus, the FT thermochronology of thermally sensitive apatite is a good tool to describe the process of basin evolution.

During the late Cretaceous, the northern and southern portions of the East Asian margin were buried by thick piles of marine sediments called the Yezo and Izumi Groups, respectively. The paleogeographic features of the Yezo sedimentary basin are difficult to interpret. For example, some paleomagnetic data obtained from the Yezo Group in Hokkaido (northern Japan) are indicative of post-Cretaceous large northward migration (Tamaki et al., 2008), whereas paleolatitudes of other areas show an affinity to the synchronous Russian data (Tamaki and Itoh, 2008). Because the pull-apart sag filled by the Izumi Group was pinned at the present latitude on the basis of a reliable paleoreconstruction of the Far East (Itoh et al., 2006), the whereabouts of the contemporaneous basins are key to refining the plate reconstruction model. However, a lack of fossils that can be efficiently used for interbasinal correlation has hindered the deciphering of the regional tectonic history recorded in those sequences.

In the present study, apatite grains separated from volcanic ash layers intercalated in the Izumi Group were investigated with the aim of precise stratigraphic correlation. Apatite is commonly found in intermediate to felsic igneous rocks and is characterized by considerable variation in its trace element composition, a characteristic that has often been used to evaluate petrogenetic processes (e.g., Piccoli and Candela, 2002; Chu et al., 2009). The accessory mineral is also noteworthy for its strong resistance to alteration and weathering (Takashima et al., 2017), which is ideal for use in establishing a chronological framework for deeply buried and exhumed pyroclastic rocks. By exploiting the physicochemical properties of apatite, the authors present a likely interpretation of evolutionary process of the Izumi Basin on the northwestern Pacific convergent margin.

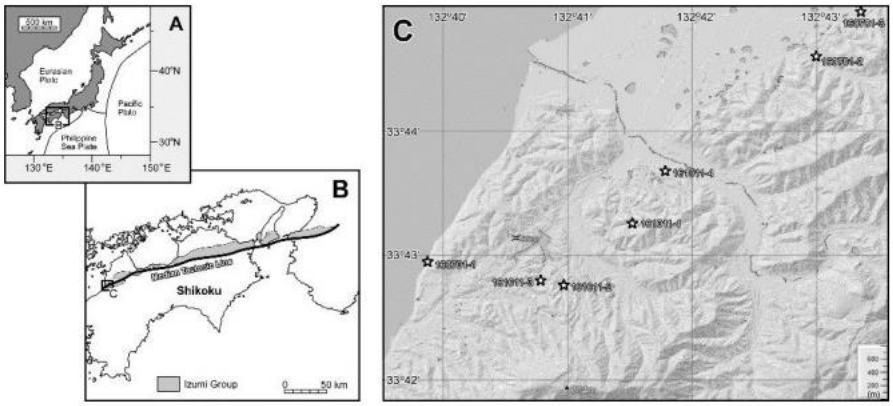

Figure 1. Sampling location index. The geologic map is adapted from the Geological Survey of Japan (2012).

2. GEOLOGICAL BACKGROUND

As summarized by Noda and Toshimitsu (2009), the subaqueous deposits of the Izumi Group are classified into peripheral and axial facies, which are composed of thick mudstones accompanied by basal conglomerates and alternating beds of turbiditic sandstone and mudstone,

respectively. They are considered to have deposited as deltas and submarine fans. The depositional age of the unit around the area of the present study (western part of Shikoku Island) ranges from early to middle Campanian (Miyazaki et al., 2016). The Izumi Group fills a 10–20-km-wide pull-apart basin on the MTL extending along the northern coast of Shikoku Island (Figure 1). Outcrop volcanic ash samples of the Izumi Group were obtained from seven sites (Figure 1). These samples are laminated light-colored fine ashes intercalated in alternating beds of sandstone and mudstone. The unit is folded with northeastward-plunging axes, and its age generally decreases toward the east.

3. Analytical Methods

As a common pretreatment for the thermo- and tephrochronological analyses, dried hand samples were crushed in a jaw crusher. The ground samples were rinsed to remove dust and processed by conventional mineral separation techniques, namely heavy liquid (e.g., liquid sodium polytungstate) and magnetic separation. Zircon grains were found in five sites (160701-1, 160701-2, 161011-1, 161011-2, and 161011-4) and were used for the FT dating. Apatites were obtained from the heavy fraction of two sites (160701-1 and 160701-2) and assessed using FT analysis for age determination and track length measurements, and electron microprobe analysis.

3.1. Fission Track Analysis

The acquired apatite grains were mounted in thermoplastic epoxy sheets set on heated glass slides. The samples were polished to reveal the internal surfaces of the crystals and then etched for 20 s in 5 M HNO_3 at room temperature (20°C) to allow the visualization of spontaneous FTs. Zircon grains were embedded in Teflon fluorinated ethylene propylene (FEP) sheets between heated microscope slides on a hot plate, polished to

expose the crystalline internal surfaces, and etched in a molten KOH–NaOH eutectic etchant at approximately 220°C for an appropriate time (10–100 h) to reveal properly etched FTs.

After the etching, all mounts were cut square to 1.5 cm × 1.0 cm, and soaked successively in detergent, alcohol, and distilled water to clean them. They were then tightly sealed in contact with low-uranium detectors made of muscovite wrapped in a heat-shrinking membrane. Each batch of mounted samples was stacked between two pieces of uranium standard glass prepared in a similar fashion. The batches were then settled in an aluminum can for neutron irradiation. The muscovite detectors were peeled away from the mounted grains and standard glasses after irradiation and then etched in hydrofluoric acid to allow the visualization of the induced tracks produced by the nuclear fission of ^{235}U, which is inherently present in the apatite/zircon and standard glass.

The FT ages were calculated based on the standard equation using the zeta calibration method (see Eq. 5 of Hurford and Green, 1983). In this study, the external detector method (EDM; Gleadow, 1981) was used for age determination; this method can be used to determine FT ages for single grains. In the case of apatite, tracks were counted in 20 grains for each mount. If 20 grains could not be obtained from a mount, all available grains were used. The number of grains used for counting depended upon the availability of suitably etched and oriented grains. Only grains that were oriented with surfaces parallel to the crystallographic *c*-axis were analyzed. Such grains were found based on the etching characteristics together with morphological evidence for euhedral grains. The grain mount was then sequentially scrutinized, and the first 20 suitably oriented objects encountered were treated as described by the following procedure.

Tracks falling within an eyepiece graticule divided into 100 grid squares were counted. The number N_s of spontaneous tracks within a certain number N_a of grid squares was recorded for each grain. Next, the number N_i of induced tracks within the corresponding locations of the muscovite external detector was recorded. The densities ρ_s and ρ_i of spontaneous and induced tracks were calculated by dividing the track counts by the total area counted, which is the product of N_a and the area of

each grid square. The FT ages were eventually determined by substituting the track counts N_s and N_i for the track densities ρ_s and ρ_i.

Neutron irradiation was carried out in a well-thermalized flux (X-7 facility; ratio of Cd to Au of approximately 98) in the High Flux Australian Reactor (HIFAR) of the Australian Atomic Energy Commission. The total neutron fluence was evaluated based on the number of tracks counted in mica external detectors attached to two pieces of Corning Glass Works standard glass CN5 (containing approximately 11 ppm U) in the irradiation canister at each end of the sample stack. Twenty-five fields were usually counted in each detector to determine the track densities within the external detectors irradiated adjacent to the uranium standard glasses. The track density ρ_D was determined by dividing the total track count N_D by the total area counted. The counted fields were arranged in a 5 × 5 grid that spanned the entire area of the detector. In the irradiation facility, a small flux gradient was occasionally observed over the length of the sample package. If a detectable gradient was present, the track count in the external detector adjacent to each standard glass was converted to a track density ρ_D, and a value for each mount in the stack was deduced through linear interpolation. When no gradient was detected, the track counts from the two external detectors were pooled to give a single value of ρ_D, which was then used to calculate the FT age for each sample.

The FT dating of apatites from deeply buried rocks revealed that the technique is extremely thermally sensitive, suggesting that FT ages may be reset at relatively low temperatures around 100°C over geological timescales (Wagner and Reimer, 1972). The integration of FT ages with confined track length measurements (Bhandari et al., 1971) has provided a deeper understanding of the analytical method. Early studies have shown that even in volcanic rocks that have experienced only moderate temperatures after initial post-eruption cooling, the mean lengths of confined tracks (approximately 14–15 μm) were less than those of induced tracks (approximately 16 μm) within the same apatites. Green (1980) presented a justification for this in terms of the thermal annealing of these tracks at low temperatures (<50°C) over prolonged geological timescales.

Confined FTs are used for track length studies in apatite. They are defined as tracks that do not intersect the polished internal surface of crystals but have been affected by etchant that has infiltrated the crystals via other tracks or fractures. In this way, the entire length of each track is securely etched. They are then measured using a digitizing tablet connected to a computer and superimposed on the field of view of a microscope via a projection tube. This system enables individual tracks to be measured with a precision of ±0.2 μm. Because of the anisotropic annealing efficiency of FTs in apatite, tracks were measured only in prismatic grains, which show sharp polishing scratches with well-etched tracks having omnidirectional narrow cone angles. According to a recommendation by Laslett et al. (1982), only horizontal tracks were measured. When possible, 100 tracks were measured per sample. For samples with a low track density and/or those in which only a limited number of apatites are obtained, it was often the case that fewer than 100 confined tracks were available. In such cases, the entire mount was scanned to detect as many confined tracks as possible.

To make realistic predictions of apatite FT parameters within geologic time scales, it is key to convert the isothermal annealing models to variable temperature models based on the natural settings (Duddy et al., 1988). The principle of equivalent time states that the annealing rate of an FT at any given time depends only on the length to which the track has already been reduced and the prevailing temperature, and not on the history of how the track reached the present length. On this basis, Green et al. (1989) developed methods for the quantitative modeling of the response of apatite FTs under various types of thermal history. Another crucial finding is that the chlorine content has a systematic influence on the annealing rate (e.g., Green et al., 1986). In practice, variation in the FT age and track length with the Cl weight content allows the identification of any anomalous grains that represent exceptional annealing properties (e.g., Crowhurst et al., 2002). Such anomalies can be eliminated from the dataset prior to the extraction of thermal history solutions.

3.2. Electron Microprobe Analysis

Apatites manually selected under a binocular microscope were mounted on small acrylate resin plates with nonsticky epoxy adhesive and then carefully polished. Because the X-ray intensity of chlorine has considerable levels of crystalline anisotropy during the microprobe analysis of apatite (Stormer et al., 1993), all the apatite grains were oriented parallel to the *c*-axis.

Twenty apatite phenocrysts from each site were analyzed in terms of their major and minor elements at the Institute for Materials Research, Tohoku University, using a JEOL 8530F wavelength dispersive electron probe microanalyzer. The analytical procedure by Gross et al. (2013) was applied with an acceleration voltage of 15 kV and a 20-nA beam current. All analysis was executed using a defocused electron beam of 10 μm in size, and the peak and background counting times per element were set to 30 and 15 s, respectively. Wavelength dispersive spectrometer calibrations for Cl, Ca, F, Mn, Y, Mg, Ce, and P were based on the JEOL standards for the determination of NaCl, CaF_2, $MnTiO_3$, $ZrYO_2$, $MgSiO_3$, and CeP_5O_{14}, respectively.

4. RESULTS

4.1. Thermal History Deduced from Fission Track Data

As mentioned above, apatite and zircon grains were obtained from two and five sites, respectively. Detailed information on the dating results is given in Tables 1–7. Regarding the thermochronological analysis of apatites from two sites, summaries of the track length measurements and a comparison of the basic analytical parameters of the two samples are presented in Tables 8 and 9, respectively.

Table 1. Details of apatite fission track dating for Sp. 160701-1.

Slide ref.	Grain #	N_s	N_i	N_a	ρ_s	ρ_i	RATIO	U (ppm)	Cl (wt%)	FT age (Ma)
G1291-5	3	4	14	32	1.986E+05	6.952E+05	0.286	5.5	0.31	79.8 ± 45.3
G1291-5	4	5	28	30	2.648E+05	1.483E+06	0.179	11.8	0.00	50.0 ± 24.3
G1291-5	5	1	8	30	5.297E+04	4.238E+05	0.125	3.4	0.24	35.0 ± 37.2
G1291-5	6	5	12	35	2.270E+05	5.448E+05	0.417	4.3	0.39	116.0 ± 61.8
G1291-5	7	3	15	25	1.907E+05	9.534E+05	0.200	7.6	0.29	56.0 ± 35.4
G1291-5	8	4	19	64	9.932E+04	4.718E+05	0.211	3.8	0.36	58.9 ± 32.4
G1291-5	9	4	12	36	1.766E+05	5.297E+05	0.333	4.2	0.40	93.0 ± 53.8
G1291-5	10	6	29	64	1.490E+05	7.200E+05	0.207	5.7	0.44	57.9 ± 26.0
G1291-5	11	0	12	35	0.000E+00	5.448E+05	0.000	4.3	0.45	0.0 ± 39.6
G1291-5	12	2	18	30	1.059E+05	9.534E+05	0.111	7.6	0.30	31.1 ± 23.2
G1291-5	13	4	23	50	1.271E+05	7.310E+05	0.174	5.8	0.30	48.7 ± 26.4
G1291-5	15	6	14	42	2.270E+05	5.297E+05	0.429	4.2	0.49	119.3 ± 58.3
G1291-5	18	6	25	49	1.946E+05	8.107E+05	0.240	6.5	0.27	67.1 ± 30.6
G1291-5	19	6	13	50	1.907E+05	4.132E+05	0.462	3.3	0.00	128.4 ± 63.5
G1291-5	20	8	39	70	1.816E+05	8.853E+05	0.205	7.1	0.27	57.4 ± 22.3
G1291-5	21	9	23	45	3.178E+05	8.122E+05	0.391	6.5	0.45	109.0 ± 43.0
G1291-5	22	6	32	60	1.589E+05	8.475E+05	0.188	6.8	0.45	52.5 ± 23.4
G1291-5	23	3	8	36	1.324E+05	3.531E+05	0.375	2.8	0.30	104.5 ± 70.8
G1291-5	24	9	35	45	3.178E+05	1.236E+06	0.257	9.9	0.37	71.9 ± 26.9
G1291-5	29	11	46	70	2.497E+05	1.044E+06	0.239	8.3	0.27	66.8 ± 22.5
G1291-5	74	48	68	18	4.238E+06	6.003E+06	0.706	47.8	0.00	195.4 ± 37.2
		150	493		2.602E+05	8.553E+05		6.8		

Area of basic unit = 6.293E-07 cm^2

χ^2 = 36.861 with 20 degrees of freedom

P (χ^2) = 1.2 %

Age disp.= 37.952 %

N_s / N_i = 0.304 ± 0.028

Mean ratio = 0.273 ± 0.033

Ages calculated using a zeta of 392.9 ± 7.4 for CN5 glass

ρ = 1.430E+06 cm^{-2} ND = 2343

ρ_D interpolated between top of can; ρ=1.378E+6cm^{-2} ND=1084

bottom of can; ρ=1.601E+6cm^{-2} ND=1259

POOLED AGE: 84.9 ± 8.3 Ma

CENTRAL AGE: 76.2 ± 10.3 Ma

Table 2. Details of apatite fission track dating for Sp. 160701-2.

Slide ref.	Grain #	N_s	N_i	N_a	ρ_s	ρ_i	RATIO	U (ppm)	Cl (wt%)	FT age (Ma)
G1290-5	3	6	23	48	1.986E+05	7.614E+05	0.261	6.1	0.17	72.4 ± 33.3
G1290-5	4	2	12	49	6.486E+04	3.892E+05	0.167	3.1	0.21	46.4 ± 35.4
G1290-5	5	3	14	50	9.534E+04	4.449E+05	0.214	3.6	0.19	59.5 ± 37.9
G1290-5	6	3	6	40	1.192E+05	2.384E+05	0.500	1.9	0.18	138.1 ± 97.7
G1290-5	8	24	75	49	7.783E+05	2.432E+06	0.320	19.5	0.02	88.7 ± 21.0
G1290-5	11	6	17	80	1.192E+05	3.377E+05	0.353	2.7	0.19	97.8 ± 46.5
G1290-5	12	8	15	48	2.648E+05	4.966E+05	0.533	4.0	0.18	147.2 ± 64.6
G1290-5	13	4	15	70	9.080E+04	3.405E+05	0.267	2.7	0.16	74.0 ± 41.7
G1290-5	14	23	80	60	6.091E+05	2.119E+06	0.287	17.0	0.04	79.7 ± 19.0
G1290-5	15	11	45	64	2.731E+05	1.117E+06	0.244	9.0	0.22	67.9 ± 22.9
G1290-5	16	5	19	36	2.207E+05	8.387E+05	0.263	6.7	0.20	73.0 ± 36.8
G1290-5	17	12	50	100	1.907E+05	7.945E+05	0.240	6.4	0.19	66.6 ± 21.5
G1290-5	19	4	16	45	1.413E+05	5.650E+05	0.250	4.5	0.21	69.4 ± 38.8
G1290-5	20	3	16	40	1.192E+05	6.356E+05	0.188	5.1	0.23	52.1 ± 32.8
G1290-5	21	4	14	36	1.766E+05	6.180E+05	0.286	5.0	0.22	79.3 ± 45.0
G1290-5	22	3	12	49	9.729E+04	3.892E+05	0.250	3.1	0.19	69.4 ± 44.8
G1290-5	23	16	33	20	1.271E+06	2.622E+06	0.485	21.0	0.93	133.9 ± 41.0
G1290-5	24	5	9	30	2.648E+05	4.767E+05	0.556	3.8	0.19	153.2 ± 85.6
G1290-5	26	5	18	100	7.945E+04	2.860E+05	0.278	2.3	0.19	77.1 ± 39.0
G1290-5	27	2	8	42	7.567E+04	3.027E+05	0.250	2.4	0.20	69.4 ± 54.9
G1290-5	29	0	13	60	0.000E+00	3.443E+05	0.000	2.8	0.20	0.0 ± 36.0
G1290-5	31	4	19	80	7.945E+04	3.774E+05	0.211	3.0	0.26	58.5 ± 32.2
G1290-5	44	6	43	70	1.362E+05	9.761E+05	0.140	7.8	0.22	38.8 ± 17.0
G1290-5	51	29	67	15	3.072E+06	7.098E+06	0.433	57.0	0.00	119.7 ± 26.8
G1290-5	58	5	17	70	1.135E+05	3.859E+05	0.294	3.1	0.18	81.6 ± 41.6
G1290-5	59	41	88	16	4.072E+06	8.740E+06	0.466	70.1	0.00	128.7 ± 24.6
		234	744		2.720E+05	8.649E+05		6.9		

Area of basic unit = 6.293E-07 cm^2

χ^2 = 23.930 with 25 degrees of freedom

P (χ^2) = 52.3 %

Age disp.= 14.739 % (did not converge)

N_s / N_i = 0.315 ± 0.024

Mean ratio = 0.297 ± 0.026

Ages calculated using a zeta of 392.9 ± 7.4 for CN5 glass

ρ = 1.421E+06 cm^{-2} ND = 2291

ρ_D interpolated between top of can; ρ=1.397E+6cm^{-2} ND=1099

bottom of can; ρ=1.515E+6cm^{-2} ND=1192

POOLED AGE: 87.2 ± 7.0 Ma

CENTRAL AGE: 85.4 ± 7.6 Ma

Table 3. Details of zircon fission track dating for Sp. 160701-1.

Slide ref.	Grain #	N_s	N_i	N_a	ρ_s	ρ_i	RATIO	Uranium (ppm)	FT age (Ma)
G1295-13	1	53	30	30	2.807E+06	1.589E+06	1.767	63.9	101.8 ± 23.4
G1295-13	2	128	80	20	1.017E+07	6.356E+06	1.600	255.7	92.3 ± 13.3
G1295-13	3	70	81	20	5.562E+06	6.436E+06	0.864	258.9	50.0 ± 8.2
G1295-13	4	89	66	30	4.714E+06	3.496E+06	1.348	140.6	77.9 ± 12.8
G1295-13	5	54	37	12	7.151E+06	4.900E+06	1.459	197.1	84.2 ± 18.1
G1295-13	8	153	150	36	6.754E+06	6.621E+06	1.020	266.4	59.0 ± 6.9
G1295-13	9	74	49	12	9.799E+06	6.489E+06	1.510	261.0	87.1 ± 16.2
G1295-13	11	88	79	20	6.992E+06	6.277E+06	1.114	252.5	64.4 ± 10.1
G1295-13	13	62	47	15	6.568E+06	4.979E+06	1.319	200.3	76.2 ± 14.8
G1295-13	19	105	79	18	9.270E+06	6.974E+06	1.329	280.6	76.8 ± 11.6
G1295-13	20	75	46	20	5.959E+06	3.655E+06	1.630	147.0	94.0 ± 17.8
G1295-13	21	79	59	20	6.277E+06	4.688E+06	1.339	188.6	77.3 ± 13.4
G1295-13	24	89	61	20	7.071E+06	4.847E+06	1.459	195.0	84.2 ± 14.1
G1295-13	26	91	81	28	5.164E+06	4.597E+06	1.123	184.9	64.9 ± 10.0
G1295-13	28	98	68	40	3.893E+06	2.701E+06	1.441	108.7	83.2 ± 13.3
G1295-13	29	59	54	30	3.125E+06	2.860E+06	1.093	115.1	63.2 ± 12.0
G1295-13	30	132	146	36	5.827E+06	6.445E+06	0.904	259.3	52.3 ± 6.4
G1295-13	31	76	52	25	4.831E+06	3.305E+06	1.462	133.0	84.4 ± 15.3
G1295-13	32	49	46	25	3.115E+06	2.924E+06	1.065	117.6	61.6 ± 12.7
G1295-13	33	56	46	25	3.560E+06	2.924E+06	1.217	117.6	70.3 ± 14.1
		1680	1357		5.539E+06	4.474E+06		180.0	

Area of basic unit = 6.293E-07 cm^2

χ^2 = 29.738 with 19 degrees of freedom

P (χ^2) = 5.5 %

Age disp.= 12.147 %

N_s / N_i = 1.238 ± 0.045

Mean ratio = 1.303 ± 0.055

Ages calculated using a zeta of 87.7 ± 0.8 for U3 glass

ρ = 1.325E+06 cm^{-2} ND = 2075

ρ_D interpolated between top of can; ρ=1.304E+6cm^{-2} ND=1026

bottom of can; ρ=1.334E+6cm^{-2} ND=1049

POOLED AGE: 71.5 ± 3.1 Ma

CENTRAL AGE: 72.5 ± 3.8 Ma

Table 4. Details of zircon fission track dating for Sp. 160701-2.

Slide ref.	Grain #	N_s	N_i	N_a	ρ_s	ρ_i	RATIO	Uranium (ppm)	FT age (Ma)
G1295-14	2	158	154	40	6.277E+06	6.118E+06	1.026	245.8	59.4 ± 6.9
G1295-14	4	227	180	30	1.202E+07	9.534E+06	1.261	383.1	72.9 ± 7.5
G1295-14	5	86	84	15	9.111E+06	8.899E+06	1.024	357.5	59.3 ± 9.2
G1295-14	7	123	76	20	9.773E+06	6.038E+06	1.618	242.6	93.5 ± 13.8
G1295-14	8	102	88	16	1.013E+07	8.740E+06	1.159	351.1	67.1 ± 9.9
G1295-14	11	104	59	20	8.263E+06	4.688E+06	1.763	188.3	101.7 ± 16.8
G1295-14	17	242	178	40	9.614E+06	7.071E+06	1.360	284.1	78.6 ± 8.0
G1295-14	18	177	186	36	7.813E+06	8.210E+06	0.952	329.9	55.1 ± 5.9
G1295-14	20	138	114	20	1.096E+07	9.058E+06	1.211	363.9	70.0 ± 9.0
G1295-14	22	89	57	15	9.428E+06	6.038E+06	1.561	242.6	90.2 ± 15.5
G1295-14	23	102	68	15	1.081E+07	7.204E+06	1.500	289.4	86.7 ± 13.7
G1295-14	24	55	55	15	5.827E+06	5.827E+06	1.000	234.1	57.9 ± 11.1
G1295-14	27	91	66	24	6.025E+06	4.370E+06	1.379	175.6	79.7 ± 13.0
G1295-14	29	101	105	20	8.025E+06	8.343E+06	0.962	335.2	55.7 ± 7.9
G1295-14	31	96	89	15	1.017E+07	9.428E+06	1.079	378.8	62.4 ± 9.3
G1295-14	32	86	75	15	9.111E+06	7.945E+06	1.147	319.2	66.4 ± 10.6
G1295-14	33	158	127	36	6.974E+06	5.606E+06	1.244	225.2	72.0 ± 8.7
G1295-14	34	128	109	25	8.136E+06	6.928E+06	1.174	278.4	68.0 ± 9.0
G1295-14	37	78	48	20	6.197E+06	3.814E+06	1.625	153.2	93.8 ± 17.4
G1295-14	38	100	74	12	1.324E+07	9.799E+06	1.351	393.7	78.1 ± 12.1
		2441	1992		8.639E+06	7.050E+06		283.2	

Area of basic unit = 6.293E-07 cm^2

χ^2 = 31.981 with 19 degrees of freedom

P (χ^2) = 3.1 %

Age disp.= 10.375 %

N_s / N_i = 1.225 ± 0.037

Mean ratio = 1.270 ± 0.054

Ages calculated using a zeta of 87.7 ± 0.8 for U3 glass

ρ = 1.327E+06 cm^{-2} ND = 2075

ρ_D interpolated between top of can; ρ=1.304E+6cm^{-2} ND=1026

bottom of can; ρ=1.334E+6cm^{-2} ND=1049

POOLED AGE: 70.9 ± 2.7 Ma

CENTRAL AGE: 71.3 ± 3.2 Ma

Table 5. Details of zircon fission track dating for Sp. 161011-1.

Slide ref.	Grain #	N_s	N_i	N_a	ρ_s	ρ_i	RATIO	Uranium (ppm)	FT age (Ma)
G1295-15	1	94	79	25	5.975E+06	5.021E+06	1.190	201.5	68.9 ± 10.6
G1295-15	4	25	21	20	1.986E+06	1.669E+06	1.190	66.9	69.0 ± 20.5
G1295-15	5	111	92	20	8.819E+06	7.310E+06	1.207	293.3	69.9 ± 10.0
G1295-15	6	35	35	16	3.476E+06	3.476E+06	1.000	139.5	58.0 ± 13.9
G1295-15	8	105	79	15	1.112E+07	8.369E+06	1.329	335.8	77.0 ± 11.6
G1295-15	9	46	35	20	3.655E+06	2.781E+06	1.314	111.6	76.1 ± 17.2
G1295-15	10	92	48	16	9.137E+06	4.767E+06	1.917	191.3	110.7 ± 19.9
G1295-15	11	53	22	16	5.264E+06	2.185E+06	2.409	87.7	138.8 ± 35.4
G1295-15	12	70	61	40	2.781E+06	2.423E+06	1.148	97.2	66.5 ± 11.8
G1295-15	14	63	62	18	5.562E+06	5.473E+06	1.016	219.6	58.9 ± 10.6
G1295-15	15	48	46	16	4.767E+06	4.569E+06	1.043	183.3	60.5 ± 12.6
G1295-15	16	73	56	25	4.640E+06	3.560E+06	1.304	142.8	75.5 ± 13.5
G1295-15	17	51	47	16	5.065E+06	4.668E+06	1.085	187.3	62.9 ± 12.8
G1295-15	18	49	40	20	3.893E+06	3.178E+06	1.225	127.5	71.0 ± 15.2
G1295-15	19	66	71	30	3.496E+06	3.761E+06	0.930	150.9	53.9 ± 9.3
G1295-15	22	66	67	25	4.195E+06	4.259E+06	0.985	170.9	57.1 ± 10.0
G1295-15	23	166	97	25	1.055E+07	6.166E+06	1.711	247.4	98.9 ± 12.9
G1295-15	25	70	41	20	5.562E+06	3.258E+06	1.707	130.7	98.7 ± 19.6
G1295-15	29	51	43	25	3.242E+06	2.733E+06	1.186	109.7	68.7 ± 14.3
G1295-15	33	94	61	16	9.336E+06	6.058E+06	1.541	243.1	89.1 ± 14.8
		1428	1103		5.352E+06	4.134E+06		165.9	

Area of basic unit = 6.293E-07 cm^2

χ^2 = 31.583 with 19 degrees of freedom

P (χ^2) = 3.5 %

Age disp.= 13.741 %

N_s / N_i = 1.295 ± 0.052

Mean ratio = 1.322 ± 0.083

Ages calculated using a zeta of 87.7 ± 0.8 for U3 glass

ρ = 1.328E+06 cm^{-2} ND = 2075

ρ_D interpolated between top of can; ρ=1.304E+6cm^{-2} ND=1026

bottom of can; ρ=1.334E+6cm^{-2} ND=1049

POOLED AGE: 75.0 ± 3.5 Ma

CENTRAL AGE: 74.4 ± 4.2 Ma

Table 6. Details of zircon fission track dating for Sp. 161011-2.

Slide ref.	Grain #	N_s	N_i	N_a	ρ_s	ρ_i	RATIO	Uranium (ppm)	FT age (Ma)
G1295-16	5	52	44	13	6.356E+06	5.378E+06	1.182	215.5	68.6 ± 14.1
G1295-16	6	48	60	20	3.814E+06	4.767E+06	0.800	191.0	46.5 ± 9.1
G1295-16	10	38	32	15	4.026E+06	3.390E+06	1.188	135.8	68.9 ± 16.6
G1295-16	15	29	22	12	3.840E+06	2.913E+06	1.318	116.7	76.4 ± 21.7
G1295-16	17	56	33	16	5.562E+06	3.277E+06	1.697	131.3	98.2 ± 21.7
G1295-16	22	46	65	16	4.569E+06	6.456E+06	0.708	258.7	41.1 ± 8.0
G1295-16	25	34	38	20	2.701E+06	3.019E+06	0.895	121.0	52.0 ± 12.3
		303	294		4.299E+06	4.171E+06		167.2	

Area of basic unit = 6.293E-07 cm^2

χ^2 = 12.761 with 6 degrees of freedom

P (χ^2) = 4.7 %

Age disp.= 20.086 %

N_s / N_i = 1.031 ± 0.084

Mean ratio = 1.112 ± 0.129

Ages calculated using a zeta of 87.7 ± 0.8 for U3 glass

ρ = 1.330E+06 cm^{-2} ND = 2075

ρ_D interpolated between top of can; ρ=1.304E+6cm^{-2} ND=1026

bottom of can; ρ=1.334E+6cm^{-2} ND=1049

POOLED AGE: 59.8 ± 5.1 Ma

CENTRAL AGE: 60.8 ± 7.0 Ma

Table 7. Details of zircon fission track dating for Sp. 161011-4.

Slide ref.	Grain #	N_s	N_i	N_a	ρ_s	ρ_i	RATIO	Uranium (ppm)	FT age (Ma)
G1295-17	2	53	40	12	7.018E+06	5.297E+06	1.325	212.0	76.9 ± 16.2
G1295-17	7	91	97	40	3.615E+06	3.853E+06	0.938	154.2	54.6 ± 8.1
G1295-17	8	25	42	15	2.648E+06	4.449E+06	0.595	178.1	34.7 ± 8.8
G1295-17	9	144	102	20	1.144E+07	8.104E+06	1.412	324.3	81.9 ± 10.8
G1295-17	11	55	43	9	9.711E+06	7.592E+06	1.279	303.8	74.3 ± 15.2
G1295-17	13	48	44	18	4.238E+06	3.884E+06	1.091	155.5	63.4 ± 13.3
G1295-17	15	74	46	18	6.533E+06	4.061E+06	1.609	162.5	93.3 ± 17.7
G1295-17	16	57	54	20	4.529E+06	4.290E+06	1.056	171.7	61.4 ± 11.7
G1295-17	17	72	71	25	4.577E+06	4.513E+06	1.014	180.6	59.0 ± 10.0
G1295-17	19	42	45	15	4.449E+06	4.767E+06	0.933	190.8	54.3 ± 11.7
G1295-17	26	97	84	40	3.853E+06	3.337E+06	1.155	133.5	67.1 ± 10.1
G1295-17	27	93	51	20	7.389E+06	4.052E+06	1.824	162.2	105.6 ± 18.6
G1295-17	28	65	38	20	5.164E+06	3.019E+06	1.711	120.8	99.1 ± 20.4
G1295-17	30	105	87	30	5.562E+06	4.608E+06	1.207	184.4	70.1 ± 10.3
G1295-17	34	130	140	30	6.886E+06	7.416E+06	0.929	296.8	54.0 ± 6.7
G1295-17	40	140	122	21	1.059E+07	9.232E+06	1.148	369.5	66.7 ± 8.4
G1295-17	42	144	100	24	9.534E+06	6.621E+06	1.440	265.0	83.6 ± 11.1
G1295-17	45	75	44	20	5.959E+06	3.496E+06	1.705	139.9	98.8 ± 18.9
G1295-17	53	49	46	15	5.191E+06	4.873E+06	1.065	195.0	61.9 ± 12.8
G1295-17	58	56	45	12	7.416E+06	5.959E+06	1.244	238.5	72.3 ± 14.6
		1615	1341		6.053E+06	5.026E+06		201.1	

Area of basic unit = 6.293E-07 cm^2

χ^2 = 37.645 with 19 degrees of freedom

P (χ^2) = 0.7 %

Age disp.= 15.202 %

N_s / N_i = 1.204 ± 0.044

Mean ratio = 1.234 ± 0.070

Ages calculated using a zeta of 87.7 ± 0.8 for U3 glass

ρ = 1.332E+06 cm^{-2} ND = 2075

ρ_D interpolated between top of can; ρ=1.304E+6cm^{-2} ND=1026

bottom of can; ρ=1.334E+6cm^{-2} ND=1049

POOLED AGE: 70.0 ± 3.1 Ma

CENTRAL AGE: 69.9 ± 3.9 Ma

Table 8. Summary of length distribution of fission tracks in apatite grains.

Sample ID	Mean track length (μm)	Standard deviation (μm)	Number of tracks (N)	Number of tracks in length intervals (μm)																			
				1	2	3	4	5	6	7	8	9	10	11	12	13	14	15	16	17	18	19	20
160701-1	12.88±0.23	2.36	107	–	–	–	–	2	–	–	–	6	1	11	16	16	14	21	13	6	1	–	–
160701-2	12.34±0.25	1.97	63	–	–	–	–	–	–	–	1	2	5	8	8	17	7	12	1	2	–	–	–

Table 9. Summary of apatite fission track analysis in two outcrop samples.

Sample ID	Present temp. (°C)	Stratigraphic age (Ma)	Measured mean track length (μm)	Predicted* mean track length (μm)	Measured fission track age (Ma)	Predicted* fission track age (Ma)
160701-1	10	72.1~83.6	12.88±0.23	14.66	76.2±10.3	76
160701-2	10	72.1~83.6	12.34±0.25	14.61	87.2± 7.0	76

*Predicted values come from the default thermal history, that is, assuming that each sample is now at its maximum temperature since deposition. The values refer only to tracks formed after deposition. Samples may contain tracks inherited from sediment provenance areas. Calculations refer to apatites within the measured compositional range for each sample.

The apatite FT analytical data for the two samples collectively define three episodes of cooling from elevated paleotemperatures that began in the following intervals: 117–71 Ma (Aptian to early Maastrichtian), 81–36 Ma (Campanian to Eocene) and 38–18 Ma (late Eocene to early Miocene). Additionally, Sp. 160701-2 contains a distinct population of apatite grains yielding older measured FT ages; these define two further cooling episodes that began in the following intervals: 193–108 Ma (early Jurassic to Albian) and 37–0 Ma (late Eocene to recent). The basic results for apatites separated from Sps. 160701-1 and 160701-2 are graphically depicted in Figures 2 and 3, respectively. On the other hand, the central age of the zircon FTs and its 2σ error suggest that they were cooled below approximately 300°C between 78 and 64 Ma, which overlaps with the Campanian depositional age range (83.6–72.1 Ma) for the sampled horizons, implying a rapidly cooled provenance contemporaneous with deposition. The tectonic context of these analytical results is fully discussed in the following section.

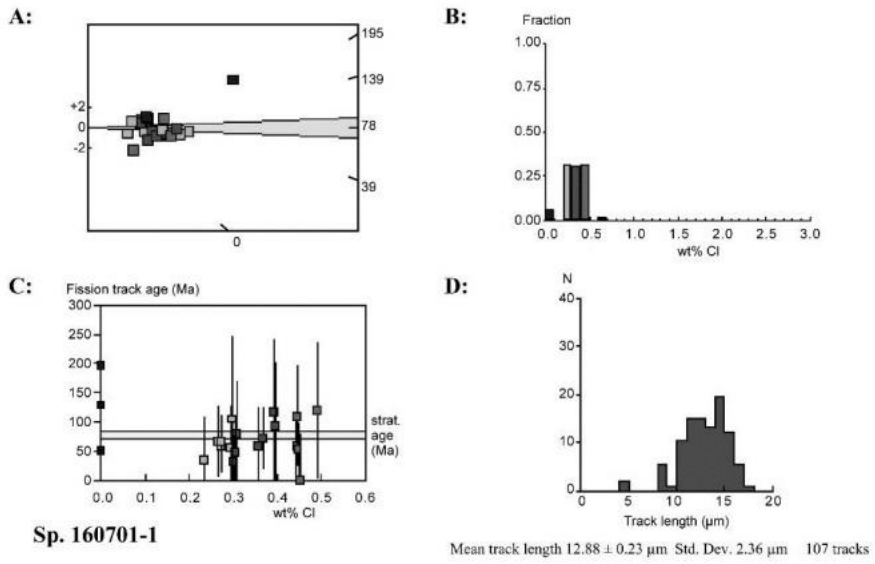

Figure 2. Fission track age data for Sp. 160701-1. A: Radial plot of single grain ages. B: Distribution of Cl content in apatite grains. C: Single-grain age versus Cl weight fraction for individual apatite grains. D: Distribution of confined track lengths.

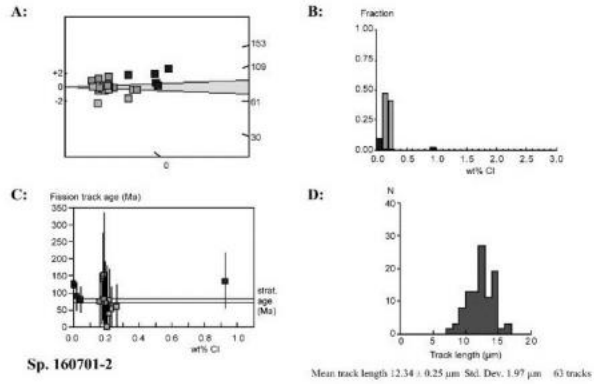

Figure 3. Fission track age data for Sp. 160701-2. A: Radial plot of single grain ages. B: Distribution of Cl content in apatite grains. C: Single-grain age versus Cl weight fraction for individual apatite grains. D: Distribution of confined track lengths.

4.2. Discrimination of Ashes Based on Apatite Trace Elements

The crystal structure of apatite is highly tolerant of structural distortion and chemical substitutions, and its trace element composition varies a great deal, reflecting the nature of the magma in which it crystallizes. Thus, the accessory mineral may be utilized to discriminate among different ashes, as much as volcanic glasses are compared based on their chemical compositions. Figure 4 shows binary plots of Cl vs. Mg, Mn vs. Fe, and Ce vs. Y for apatites from the Izumi Group. The present results strongly suggest that these simple plots are sufficient to discriminate among different volcanic ashes.

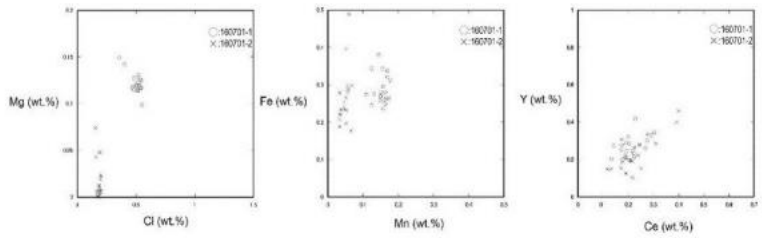

Figure 4. Binary plots of Cl vs. Mg, Mn vs. Fe, and Ce vs. Y for apatites separated from two types of volcanic ash intercalated in the Izumi Group.

5. DISCUSSION

The results of the present tephrochronological study indicate that two ashes from which affluent apatite grains were obtained originated from different host magmas. Therefore, the FT analysis results for these apatites represent independent thermal histories. Figures 5 and 6 show the burial and exhumation processes reconstructed for apatites separated from Sps. 160701-1 and 160701-2, respectively. To obtain these graphical representations, simulations were conducted using an in-house numerical Geotrack model for the analytical system, and a range of conditions was defined to provide predictions consistent with the actual data with a 95% confidence interval, as depicted by Green and Duddy (2010). The present analysis results indicate that the evidence of higher temperatures in the past was not obtained from the FT age but instead from the track length distribution (see Tables 8 and 9, and Figures 2 and 3), which means that heating associated with basin subsidence and burial was not sufficiently severe to reduce the FT age below the depositional age.

The high-quality apatite FT data (21 grain ages and 107 track lengths) of Sp. 160701-1 point to an interpretation that can be regarded as highly reliable. Though the single-grain FT ages in Sp. 160701-2 appear to follow a unimodal distribution, a detailed inspection of the data revealed that the sample consists of grains from two distinct sources. Namely, three apatite grains containing between 0.0 and 0.1 wt% Cl and with notably higher uranium contents than most of the grains define a pooled age of 105 ± 11 Ma, whereas the majority, containing between 0.1 and 0.3 wt% Cl, defines a pooled age of 70 ± 8 Ma, which is significantly younger. The low-Cl grains, as well as one grain that contains a much higher Cl content (0.93 wt%), are therefore interpreted to represent a distinct population of apatites likely derived from a basement terrane, whereas those grains containing between 0.1 and 0.3 wt% Cl are likely to represent the primary volcanic provenance. In combination, the data obtained from the four grains with anomalous Cl concentrations define a single population with a pooled FT age of 116 ± 13 Ma and a mean track length of 12.0 ± 0.4 μm (based on 15

track length measurements). These two populations were treated separately during the advanced interpretation of the present results.

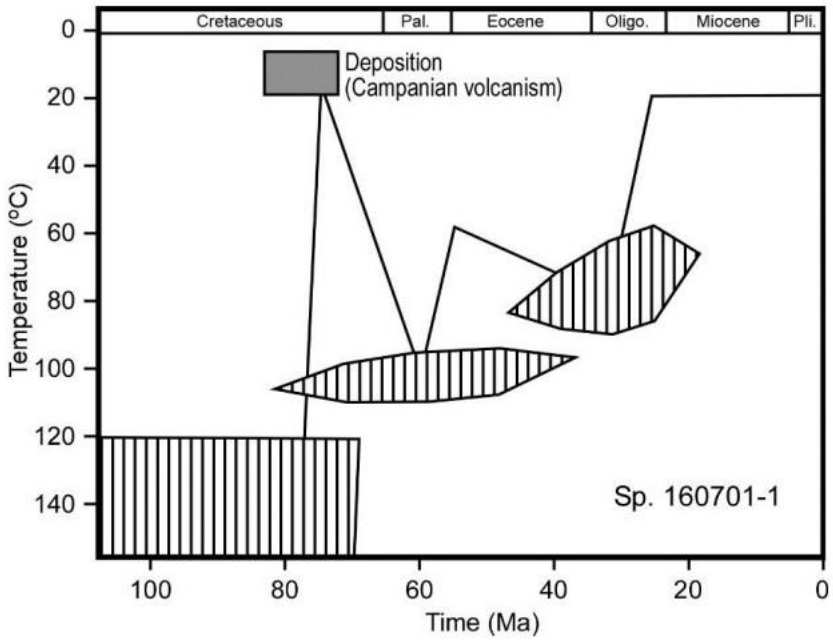

Figure 5. Thermal history interpretation of apatite FT analytical data for Sp. 160701-1. Hatched polygons represent the 95% confidence limits of the time–temperature estimates of significant events.

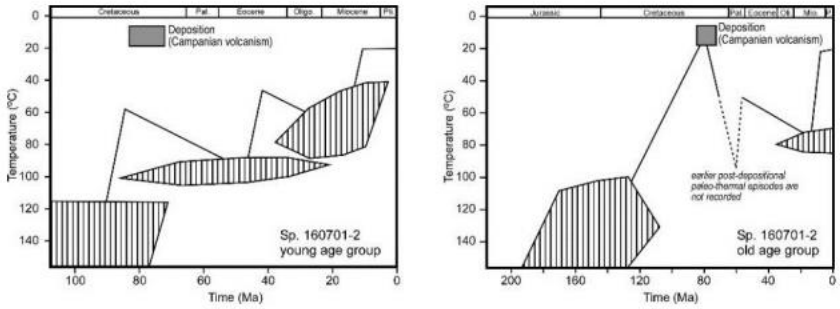

Figure 6. Thermal history interpretation of apatite FT analytical data for Sp. 160701-2. Hatched polygons represent the 95% confidence limits of the time–temperature estimates of significant events.

Figure 7 illustrates the integrated thermal history reconstruction for the volcanic ash samples based on the apatite and zircon FT analytical data presented above. The zircon analysis and most aspects of the apatite analysis in the five samples are highly consistent with a common thermal history interpretation. The zircon data indicate cooling from above 300°C around the interval 78–64 Ma, suggesting the origin of the accessory mineral from contemporaneous volcanism. All of the apatite data from Sp. 160701-1 and most such data from Sp. 160701-2 define cooling from above 115°C in the interval 117–71 Ma, which overlaps with both the time of cooling obtained from the zircon data and the depositional age of the host sediments. It was also interpreted in terms of the derivation of the apatites from contemporaneous volcanic activity excluding a minor group derived from an older provenance (not presented in Figure 7). With the older group omitted, the timing constraints obtained by the apatite and zircon analyses overlap in the range of 78–71 Ma, which provides an excellent match to the Campanian depositional age (83.6–72.1 Ma) assigned to the Izumi Group. Thus, the data support a contemporaneous volcanic origin for the majority of analyzed apatites and zircons from these samples.

The apatite FT data indicate two post-depositional episodes: 81–36 and 38–18 Ma. These are interpreted periods of heating due to a greater depth of burial and cooling due to exhumation (uplift and erosion), respectively. The older episode from the Campanian to the Eocene may be related with a regional unconformity around the K/T gap (e.g., Ando, 2003), whereas the younger one from the late Eocene to the early Miocene is synchronous with the backarc rifting event of the Japan Sea, which inevitably provoked a prevailing uplift (e.g., Itoh et al., 2006). It is noteworthy that an extensive inversion occurred around the late Miocene, which was identified in an earlier FT thermochronological study of the easternmost portion of the Izumi Group (Itoh et al., 2017b). Although the regional contraction event is probably linked to the resumed subduction of the Philippine Sea Plate, the spatiotemporal diversity of compressive stress around the southwestern Japan arc has been detected in previous studies (Itoh et al., 2014; Itoh, 2015). The paleothermal reconstruction of the present study may reflect the

delayed prevalence of the latest compressive regime around the western part of southwest Japan.

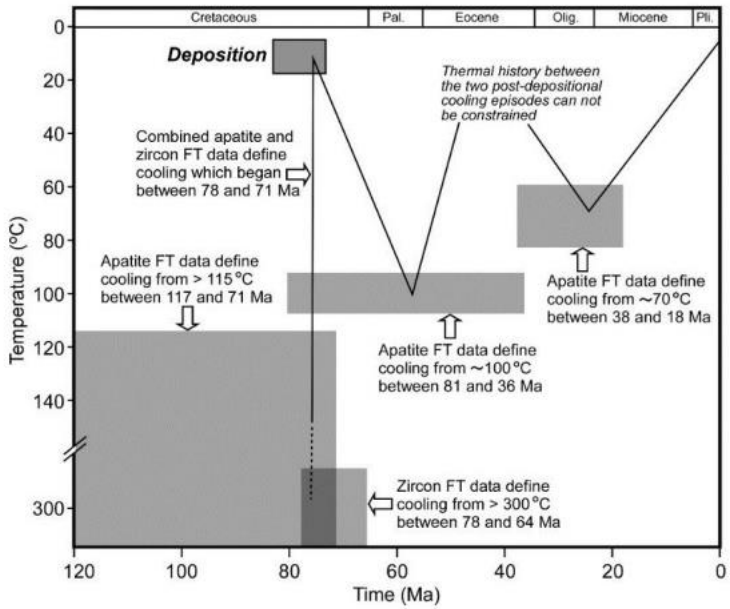

Figure 7. Integrated thermal history reconstruction of apatite and zircon data for five outcrop volcanic ash layers of the Izumi Group in southwestern Japan. In the apatite analysis, thermal events were interpreted not from the FT ages but from the track length distribution. In the zircon analysis, the cooling interval (78–64 Ma) was obtained from the 2σ uncertainty of the weighted mean age.

CONCLUSION

A well-organized tephro-/thermochronological investigation of a Cretaceous event sedimentary sequence adjacent to an arc-bisecting fault on the East Asian convergent margin was conducted. The main points of this study are summarized as follows.

1) Excellent yields of apatite and zircon were obtained from two volcanic ash samples of the Izumi Group along the MTL fault system, resulting in high-quality analytical data; thus, the

interpretations made in this study are regarded as highly reliable. Zircon grains were also extracted from three other auxiliary ashes and used to obtain FT dating results.

2) On the basis of binary plots of the trace elements (Cl vs. Mg, Mn vs. Fe, Ce vs. Y) in the apatites, it was concluded that the two ashes intercalated in the Izumi Group originated from different host magmas, which suggests that the apatite FT analysis results of the two samples represent independent thermal histories.
3) A detailed inspection of the chlorine content of apatite grains in an ash sample revealed that they were derived from two distinct sources. The minor group with greater FT ages, which likely has a basement terrane provenance, showed two cooling episodes that began in the following intervals: 193–108 Ma (early Jurassic to Albian) and 37–0 Ma (late Eocene to recent).
4) The apatite FT analysis of the major group from the two samples indicated three episodes of cooling from elevated paleotemperatures. The cooling was found to begin in the following intervals.

   117–71 Ma: Aptian to early Maastrichtian, from greater than 115°C

   81–36 Ma: Campanian to Eocene, from approximately 100°C

   38–18 Ma: late Eocene to early Miocene, from approximately 70°C
5) Zircon FT data from five sites suggest that the grains were cooled below approximately 300°C between 78 and 64 Ma, which overlaps the Campanian depositional age range for the sampled horizons, implying a rapidly cooled provenance contemporaneous with deposition.
6) In summary, two volcanic ash samples were analyzed and found to show a record of two post-depositional episodes: 81–36 and 38–18 Ma. The older episode from the Campanian to the Eocene may be related to a regional unconformity around the K/T gap, whereas the younger one from the late Eocene to the early Miocene is

synchronous with the backarc rifting of the Japan Sea, which provoked a prevailing uplift.

ACKNOWLEDGMENTS

This study was financially supported by the Comprehensive Research Project for the Beppu–Haneyama Fault Zone (Eastern Part of Oita Heiya–Yufuin Fault Zone) (FY2014-2016) organized by the Ministry of Education, Culture, Sports, Science and Technology, and Kyoto University.

REFERENCES

Ando, H. (2003). Stratigraphic correlation of Upper Cretaceous to Paleocene forearc basin sediments in Northeast Japan: cyclic sedimentation and basin evolution. *Journal of Asian Earth Sciences,* 21, 921-935.

Bhandari, N., Bhat, S. G., Lal, D., Rajagopalan, G., Tamhane, A.S., & Venkatavaradan, V.S. (1971). Fission fragment tracks in apatite: recordable track lengths. *Earth and Planetary Science Letters,* 13, 191-199.

Chu, M. F., Wang, K. L., Griffin, W. L., Chung, S. L., O'Reilly, S. Y., Pearson, N. J., & Iizuka, Y. (2009). Apatite composition: tracing petrogenetic processes in Transhimalayan Granitoids. *Journal of Petrology*, 50, 1829-1855. http://dx.doi.org/10.I0931093/petrology/egp054.

Crowhurst, P. V., Green, P. F., & Kamp, P. J. J. (2002). Appraisal of (U-Th)/He apatite thermochronology as a thermal history tool for hydrocarbon exploration: an example from the Taranaki Basin, New Zealand. *AAPG Bulletin,* 86, 1801-1819.

Duddy, I. R., Green, P. F., & Laslett, G. M. (1988). Thermal annealing of fission tracks in apatite 3 - Variable temperature behaviour. *Chemical Geology* (Isotope Geoscience Section), 73, 25-38.

Geological Survey of Japan (2012). Seamless Digital Geological Map of Japan 1:200,000 (July 3, 2012 Version), *Research Information Database DB084*. Tsukuba: Geological Survey of Japan, AIST.

Gleadow, A. J. W. (1981). Fission track dating methods: what are the real alternatives? *Nuclear Tracks,* 5, 3-14.

Green, P. F. (1980). On the cause of the shortening of spontaneous fission tracks in certain minerals. *Nuclear Tracks,* 4, 91-100.

Green, P. F., & Duddy, I. R. (2010). Synchronous exhumation events around the Arctic including examples from Barents Sea and Alaska North Slope. In B.A. Vining, & S.C. Pickering (Eds.), Petroleum Geology, from Mature Basins to New Frontiers. *Proceedings of the 7th Petroleum Geology Conference.* London: The Geological Society, pp. 633-644. doi:10.1144/0070633.

Green, P. F., Duddy, I. R., Gleadow, A. J. W., Tingate, P. R., & Laslett, G. M. (1986). Thermal annealing of fission tracks in apatite 1 - A qualitative description. *Chemical Geology* (Isotope Geoscience Section), 59, 237-253.

Green, P. F., Duddy, I. R., Laslett, G. M., Hegarty, K. A., Gleadow, A. J. W., & Lovering, J. F. (1989). Thermal annealing of fission tracks in apatite 4 - Quantitative modelling techniques and extension to geological timescales. *Chemical Geology* (Isotope Geoscience Section), 79, 155-182.

Gross, J., Filiberto, J., & Bell, A. S. (2013). Water in the martian interior: evidence for terrestrial MORB mantle-like volatile contents from hydroxyl-rich apatite in olivine-phyric shergottite NWA 6234. *Earth and Planetary Science Letters,* 369-370, 120-128.

Hurford, A. J., & Green, P. F. (1983). The zeta age calibration of fission track dating. *Isotope Geoscience,* 1, 285-317.

Itoh, Y. (2015). *Gunchu Formation - An Indicator of Active Tectonics on an Oblique Convergent Margin.* Saarbrucken: LAP LAMBERT Academic Publishing, 76 pp.

Itoh, Y., & Takashima, R. (2017). Cretaceous research: paleolatitudes and northward migration of crustal fragments in the NW Pacific inferred from paleomagnetic studies. In Y. Itoh (Ed.), *Dynamics of Arc Migration and Amalgamation - Architectural Examples from the NW Pacific Margin*. Rijeka: InTech. http://dx.doi.org/10.5772/67359.

Itoh, Y., Green, P. F., Takemura, K., & Iwata, T. (2017b). Fission track thermochronology of Late Cretaceous sandstones of the Izumi Group adjacent to the Median Tectonic Line active fault system in southwest Japan. In Y. Itoh (Ed.), *Evolutionary Models of Convergent Margins - Origin of Their Diversity.* Rijeka: InTech. http://dx.doi.org/10.5772/67962.

Itoh, Y., Kusumoto, S., & Takemura, K. (2014). Evolutionary process of Beppu Bay in central Kyushu, Japan: a quantitative study of the basin-forming process controlled by plate convergence modes. *Earth, Planets and Space,* 66, 74. doi:10.1186/1880-5981-66-74.

Itoh, Y., Takano, O., & Takashima, R. (2017a). Tectonic synthesis: a plate reconstruction model of the NW Pacific region since 100 Ma. In Y. Itoh (Ed.), *Dynamics of Arc Migration and Amalgamation - Architectural Examples from the NW Pacific Margin*. Rijeka: InTech. http://dx.doi.org/10.5772/67358.

Itoh, Y., Uno, K., & Arato, H. (2006). Seismic evidence of divergent rifting and subsequent deformation in the southern Japan Sea, and a Cenozoic tectonic synthesis of the eastern Eurasian margin. *Journal of Asian Earth Sciences,* 27, 933-942.

Laslett, G. M., Kendall, W. S., Gleadow, A. J. W., & Duddy, I. R. (1982). Bias in measurement of fission track length distributions. *Nuclear Tracks,* 6, 79-85.

Miyazaki, K., Wakita, K., Miyashita, Y., Mizuno, K., Takahashi, M., Noda, A., Toshimitsu, S., Sumii, T., Ohno, T., Nawa, K., & Miyawaka, A. (2016). Geological Map of Japan 1:200,000, Matsuyama (2nd Edition). *Tsukuba: Geological Survey of Japan, AIST.*

Noda, A., & Toshimitsu, S. (2009). Backward stacking of submarine channel-fan successions controlled by strike-slip faulting: The Izumi

Group (Cretaceous), southwest Japan. *Lithosphere,* 1, 41-59. doi:10.1130/L19.1.

Piccoli, P., & Candela, P. (2002). Apatite in igneous systems. In M. Kohn, J. Rakovan, & J. Hughes (Eds.), Phosphates - Geochemical, Geobiological, and Materials Importance, *Reviews in Mineralogy and Geochemistry* v48, pp. 255-292.

Stormer, J., Pierson, M., & Tacker, R. (1993). Variation of F and Cl X-ray intensity due to anisotropic diffusion in apatite during electron microprobe analysis. *American Mineralogists,* 78, 641-648.

Takashima, R., Kuwabara, S., Sato, T., Takemura, K., & Nishi, H. (2017). Utility of trace elements in apatite for discrimination and correlation of Quaternary ignimbrites and co-ignimbrite ashes, *Japan. Quaternary Geochronology*. http://dx.doi.org/10.1016/j.quageo.2017.04.001.

Tamaki, M., & Itoh, Y. (2008). Tectonic implications of paleomagnetic data from upper Cretaceous sediments in the Oyubari area, central Hokkaido, Japan. *Island Arc*, 17, 270-284.

Tamaki, M., Oshimbe, S., & Itoh, Y. (2008). A large latitudinal displacement of a part of Cretaceous forearc basin in Hokkaido, Japan: paleomagnetism of the Yezo Supergroup in the Urakawa area. *Journal of the Geological Society of Japan,* 114, 207-217.

Wagner, G. A., & Reimer, G. M. (1972). Fission track tectonics: the tectonic interpretation of fission track ages. *Earth and Planetary Science Letters,* 14, 263-268.